Bulk shear-mode contribution to thermally generated capillary waves on a room-temperature ionic-liquid surface

Y. Ohmasa*
Department of Intelligent Mechanical Engineering, Faculty of Engineering, Hiroshima Institute of Technology, Hiroshima 731-5193, Japan

T. Hoshino, R. Osada, and M. Yao
Department of Physics, Graduate School of Science, Kyoto University, Kyoto 606-8502, Japan
(Received 26 December 2008; revised manuscript received 6 April 2009; published 9 June 2009)

In the present work, we show that the autocorrelation function of the capillary-wave displacement is expressed by the sum of the ordinary oscillator and the bulk shear-mode terms. The former is expressed by a simple damped oscillator form or a sum of exponentially damping functions depending on the extent of damping. The latter is also written by superposition of exponentially damping modes, and an analytically exact formulation is obtained. We performed surface dynamic light-scattering experiment for the surface of an ionic liquid, 1-butyl- 3-methylimidazolium bis[(trifluoromethyl)sulfonyl]imide, and compared the experimental autocorrelation function with the theoretical one. We observed for the first time the bulk shear-mode contribution, and confirmed that the experimental data is well explained by the theoretical autocorrelation function.

DOI: 10.1103/PhysRevE.79.061601 PACS number(s): 68.03.Kn, 47.35.Pq, 78.35.+c

I. INTRODUCTION

Surface dynamic light scattering (SDLS) is a powerful nonperturbative technique to study thermally excited capillary waves (CW) on liquid surfaces [1]. Since the evolution of CW is governed by surface tension and by surface and bulk viscoelasticity, precise treatment of SDLS data allows the determination of these valuables.

The basic understanding of thermally excited CW is well established. The CW modes obey the linearized Navier-Stokes equation [2,3], and its actual thermal population is calculated by the fluctuation-dissipation theorem [4]. In the two extreme cases of low and high damping, the CW spectrum consists simply of Lorentzian lines. However, such a simple result no longer holds in intermediate damping conditions. The origin of the spectral shape modification from Lorentzian is physically interpreted as resulting from a coupling between the surface motion and the motion that it induces in the fluid underneath [5]. In intermediate damping conditions, it is important to take the non-Lorentzian aspect into account for the purpose of obtaining precise liquid parameters such as surface tension and viscosity. To our knowledge, however, there is no experimental work which takes the influence of the bulk mode in an explicit manner separately from the surface oscillator mode.

One of the most important classes of liquids which satisfy the intermediate damping condition is ionic liquids (ILs). Recently, ILs have received considerable interests for various applications such as solvents in chemical synthesis [6] and electrolytes in batteries [7] and solar cells [8]. ILs are highly viscous liquids at room temperature, but its viscosity decreases considerably when the temperature is increased. It is found recently that the CW spectra on the surface of ILs show the transition from oscillating to overdamped behavior [9–11]. Near the transition region, the non-Lorentzian aspect dominates the CW spectra, and its precise calculation is crucial in order to get liquid parameters such as surface tension and viscosity.

In a previous paper [9], we analyzed the SDLS data of an IL, 1-butyl- 3-methylimidazolium bis[(trifluoromethyl)sulfonyl]imide (hereafter abbreviated as [bmim][TFSI]) on the basis of the frequency-domain analysis using the strict theoretical expression for the power spectrum [Eq. (5) shown below]. This method gives precise liquid parameters. However, in this method, the physical interpretation of the data is not clear because it is difficult to decompose the experimental spectra into contributions of various modes. On the other hand, we analyzed the SDLS data of various ILs using the time-domain analysis in [11], and found that there exist slow and fast damping modes in the overdamped regime near the critical damping condition. In the time-domain analysis, it is easy to decompose the experimental data into modes and to obtain various parameters characterizing these modes, such as the frequency and the damping rate. In [11], we obtained dispersion relations for the slow and fast damping modes for the first time.

In the present work, we study the shape of the time-domain SDLS data in more detail. We show that the autocorrelation function of the CW displacement can be separated into ordinary oscillator and bulk shear-mode terms. The former can be expressed by a simple damped oscillator form or a sum of exponentially damping functions depending on the extent of damping. The latter is also written by a superposition of exponentially damping modes, and an analytically exact formula is obtained. The bulk shear-mode term was ignored in the previous paper [11] because it is negligibly small in the overdamped region near the critical damping. However, it becomes important in the damped oscillator side of the transition region as shown below.

This paper is organized as follows. In Sec. II, we review the theoretical background of the general description of the CW, and show that the autocorrelation function is separated into the ordinary oscillator and the bulk shear-mode terms. In

*ohmasa@cc.it-hiroshima.ac.jp

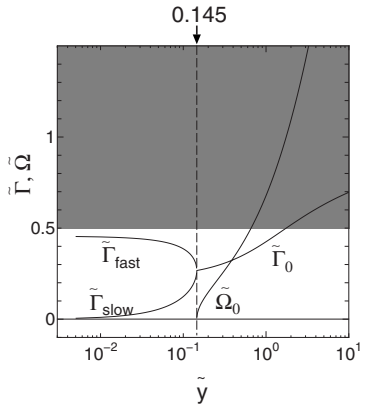

FIG. 1. Theoretical dispersion relation of capillary waves. $\tilde{\Omega}_0$ and $\tilde{\Gamma}_0$ are the dimensionless angular frequency and the damping rate in the damped oscillation region ($\tilde{y}>0.145$), respectively. $\tilde{\Gamma}_{\text{slow}}$ and $\tilde{\Gamma}_{\text{fast}}$ are the dimensionless damping rates of the slow and the fast modes in the overdamped region ($\tilde{y}<0.145$). Here, $\tilde{y}$ is a dimensionless parameter defined by the Eq. (7). The shaded area indicates the distribution of dimensionless damping rates $\tilde{\gamma}$ of bulk shear modes, which contribute to integral (19).

Sec. III, we compare the theoretical expression with the SDLS experimental data obtained on the surface of an IL, [bmim][TFSI]. Conclusions are given in Sec. IV.

II. THEORETICAL BACKGROUND

A. General description of capillary wave

We define that the liquid is filling the half space $z<0$ and its surface extends in the xy plane. Let $\zeta(x,y,t)$ denote the vertical displacement of the surface element at time t, and $\boldsymbol{v}(x,y,z,t)$ denote the velocity field in the liquid. They are related to each other as

$$v_z(z=0) \simeq \frac{\partial \zeta}{\partial t}.$$

We consider surface waves of wave vector q propagating in the x direction,

$$\boldsymbol{v} = \boldsymbol{v}_0(z)\exp[i(qx-\omega t)].$$

In the case of incompressible Newtonian liquid, the motion of the liquid is governed by the linearized Navier-Stokes equations,

$$\rho\frac{\partial \boldsymbol{v}}{\partial t} = \eta\nabla^2\boldsymbol{v} - \nabla p \tag{1}$$

and

$$\text{div}\ \boldsymbol{v} = 0, \tag{2}$$

where ρ is the density, η is the viscosity, and p is the pressure.

The solution of Eqs. (1) and (2) which satisfies the conditions

$$\boldsymbol{v}(z\to-\infty)\to 0,\ \ p(z\to-\infty)\to 0$$

is given by [2,3]

$$p = (i\omega\rho/q)Ae^{qz}e^{i(qx-\omega t)},$$

$$v_x = i\left(Ae^{qz} + \frac{m}{q}Be^{mz}\right)e^{i(qx-\omega t)},$$

$$v_y = 0,$$

$$v_z = (Ae^{qz} + Be^{mz})e^{i(qx-\omega t)}, \tag{3}$$

where A and B are constants, and $m=\sqrt{q^2-i\omega\rho/\eta}$ with $\text{Re}(m)>0$.

In addition, the motion must satisfy boundary conditions that express the continuity of the normal and tangential stresses at the surface,

$$\eta\left(\frac{\partial v_x}{\partial z} + \frac{\partial v_z}{\partial x}\right) = 0,$$

$$2\eta\frac{\partial v_z}{\partial z} - p = \sigma\frac{\partial^2\zeta}{\partial x^2},$$

where σ is the surface tension. From these conditions, the dispersion relation is obtained as [2,3]

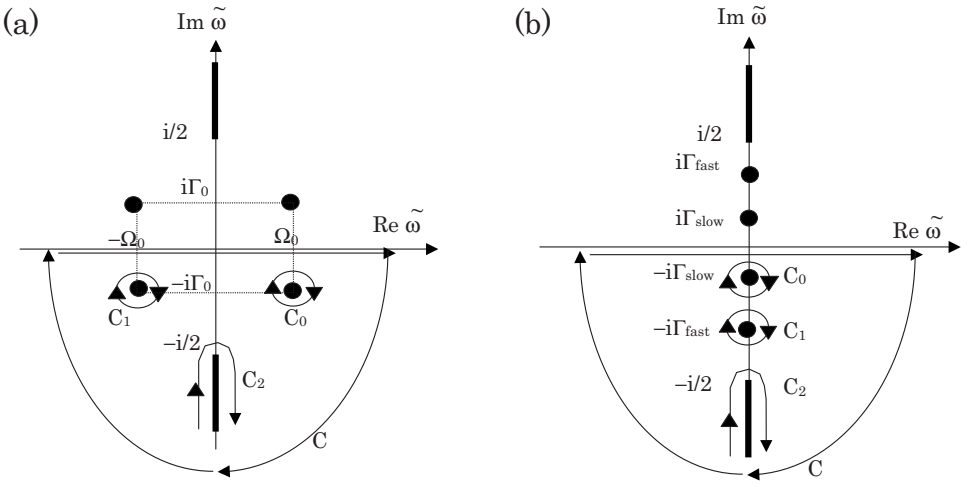

FIG. 2. Integral paths C_0, C_1, and C_2 for Fourier transformation (12) in the (a) damped oscillator region and the (b) overdamped region.

$$D(q,\omega) = (2\eta q^2/\rho)^2 m/q - (i\omega - 2\eta q^2/\rho)^2 - \sigma q^3/\rho = 0. \tag{4}$$

The power spectrum $P_T(q,\omega)$ of thermally excited capillary waves of the liquid surface is given by the fluctuation-dissipation theorem [4],

$$P_T(q,\omega) = -\frac{2k_BTq}{\rho\omega}\mathrm{Im}\frac{1}{D(q,\omega)}. \tag{5}$$

It is known that this spectrum deviates from Lorentzian in the intermediate damping region [5].

Hereafter, we use the following dimensionless variables for simplicity:

$$\tilde{\omega} = \frac{\rho}{2\eta q^2}\omega, \tag{6}$$

$$\tilde{y} = \frac{\rho\sigma}{4\eta^2 q}, \tag{7}$$

$$\tilde{t} = \frac{2\eta q^2}{\rho}t, \tag{8}$$

$$\tilde{D}(\tilde{y},\tilde{\omega}) = (\rho/2\eta q^2)^2 D(q,\omega) = (1-2i\tilde{\omega})^{1/2} - (1-i\tilde{\omega})^2 - \tilde{y}. \tag{9}$$

The variables with tilde denote the dimensionless counterparts of the dimensioned variables. Using these dimensionless variables, Eq. (5) can be rewritten as

$$P_T(q,\omega) = -\left(\frac{k_BT\rho^2}{4\eta^3 q^5}\right)\frac{1}{\tilde{\omega}}\mathrm{Im}\frac{1}{\tilde{D}(\tilde{y},\tilde{\omega})}.$$

In general, the dispersion equation

$$\tilde{D}(\tilde{y},\tilde{\omega}) = 0 \tag{10}$$

has two complex roots $\tilde{\omega}_0$ and $\tilde{\omega}_1$. When (i) $\tilde{y} > 0.145$ (damped oscillation region), the two roots have the form $\pm\tilde{\Omega}_0 - i\tilde{\Gamma}_0$. Here, $\tilde{\Omega}_0$ and $\tilde{\Gamma}_0$ are the dimensionless counterparts of the angular frequency Ω_0 and the damping rate Γ_0 of the CW, respectively. When (ii) $\tilde{y} < 0.145$ (overdamped region), the roots have pure imaginary values $-i\tilde{\Gamma}_{\mathrm{slow}}$ and $-i\tilde{\Gamma}_{\mathrm{fast}}$ ($\tilde{\Gamma}_{\mathrm{slow}} < \tilde{\Gamma}_{\mathrm{fast}}$). $\tilde{\Gamma}_{\mathrm{slow}}$ and $\tilde{\Gamma}_{\mathrm{fast}}$ are the dimensionless damping rates of slow and fast CW modes. Analytic forms of these roots have been given by Byrne and Earnshaw [12]. Figure 1 shows the $\tilde{y}$ dependence of $\tilde{\Omega}_0$, $\tilde{\Gamma}_0$, $\tilde{\Gamma}_{\mathrm{slow}}$, and $\tilde{\Gamma}_{\mathrm{fast}}$. When $\tilde{y}$ is decreased, $\tilde{\Omega}_0$ decreases and vanishes at the critical value $\tilde{y}=0.145$, where critical damping takes place. When $\tilde{y}$ is decreased below 0.145, $\tilde{\Gamma}_0$ is bifurcated into $\tilde{\Gamma}_{\mathrm{slow}}$ and $\tilde{\Gamma}_{\mathrm{fast}}$ branches.

We define the autocorrelation function $F(q,t) = \langle\zeta(q,t)\zeta(q,0)\rangle$ of Fourier components $\zeta(q,t)$ of the vertical displacement $\zeta(x,y,t)$. It is calculated by Fourier transforming $P_T(q,\omega)$ as follows:

$$\begin{aligned} F(q,t) &= \int_{-\infty}^{\infty}\frac{d\omega}{2\pi}P_T(q,\omega)e^{-i\omega t} \\ &= -F_0\tilde{y}\int_{-\infty}^{\infty}\frac{d\tilde{\omega}}{\pi}\frac{e^{-i\tilde{\omega}\tilde{t}}}{\tilde{\omega}}\mathrm{Im}\frac{1}{\tilde{D}(\tilde{y},\tilde{\omega})} \\ &= -F_0\tilde{y}\int_{-\infty}^{\infty}d\tilde{\omega}\frac{e^{-i\tilde{\omega}\tilde{t}}}{2\pi i\tilde{\omega}}\left(\frac{1}{\tilde{D}(\tilde{y},\tilde{\omega})} - \frac{1}{\tilde{D}(\tilde{y},\tilde{\omega})^*}\right), \end{aligned} \tag{11}$$

where

$$F_0 = F(q,0) = \langle|\zeta_q(t)|^2\rangle = \frac{k_BT}{\sigma q^2}.$$

is the total amplitude of the CW with wave number q.

When $\tilde{t} > 0$, the integral path should be closed in the lower half plane as indicated by the path C in Figs. 2(a) and 2(b). This integral path is decomposed into three contributions C_0, C_1, and C_2. C_0 and C_1 are the integrals around the two poles $\tilde{\omega}_0$ and $\tilde{\omega}_1$, and C_2 is around the branch cut which extends along the negative imaginary $\tilde{\omega}$ axis from $-1/2$ to $-\infty$. Because $1/\tilde{D}^*$ is analytic in the lower half plane, only the $1/\tilde{D}$ term contributes to the integral,

$$F(q,t) = -F_0\tilde{y}\left(\int_{C_0} + \int_{C_1} + \int_{C_2}\right)d\tilde{\omega}\frac{e^{-i\tilde{\omega}\tilde{t}}}{2\pi i\tilde{\omega}\tilde{D}(\tilde{y},\tilde{\omega})} \tag{12}$$

B. Ordinary oscillator term

The integrals around the paths C_0 and C_1 correspond to ordinary oscillator terms. These integrals give different functional forms depending on the value of $\tilde{y}$.

(i) In the damped oscillation region ($\tilde{y} > 0.145$), the integrals around C_0 and C_1 give an oscillatory function with the dimensionless frequency $\tilde{\Omega}_0$ and the damping rate $\tilde{\Gamma}_0$. We denote this term by $F_{\mathrm{osc}}(q,t)$,

$$\begin{aligned} F_{\mathrm{osc}}(q,t) &= -F_0\tilde{y}\left(\int_{C_0} + \int_{C_1}\right)d\tilde{\omega}\frac{e^{-i\tilde{\omega}\tilde{t}}}{2\pi i\tilde{\omega}\tilde{D}(\tilde{y},\tilde{\omega})} \\ &= \lim_{\tilde{\omega}\to-\tilde{\Omega}_0-i\tilde{\Gamma}_0}\frac{F_0\tilde{y}e^{-i\tilde{\omega}\tilde{t}}}{\tilde{\omega}\tilde{D}(\tilde{y},\tilde{\omega})}(\tilde{\omega}-\tilde{\Omega}_0+i\tilde{\Gamma}_0) \\ &\quad + \lim_{\tilde{\omega}\to-\tilde{\Omega}_0-i\tilde{\Gamma}_0}\frac{F_0\tilde{y}e^{-i\tilde{\omega}\tilde{t}}}{\tilde{\omega}\tilde{D}(\tilde{y},\tilde{\omega})}(\tilde{\omega}+\tilde{\Omega}_0+i\tilde{\Gamma}_0) \\ &= \left.\frac{F_0\tilde{y}e^{-i\tilde{\omega}\tilde{t}}}{\tilde{\omega}(d\tilde{D}/d\tilde{\omega})}\right|_{\tilde{\omega}=\tilde{\Omega}_0-i\tilde{\Gamma}_0} + \left.\frac{F_0\tilde{y}e^{-i\tilde{\omega}\tilde{t}}}{\tilde{\omega}(d\tilde{D}/d\tilde{\omega})}\right|_{\tilde{\omega}=-\tilde{\Omega}_0-i\tilde{\Gamma}_0} \\ &= \frac{A}{2}e^{-i\phi}e^{(-i\tilde{\Omega}_0-\tilde{\Gamma}_0)\tilde{t}} + (\mathrm{c.c.}) = Ae^{-\tilde{\Gamma}_0\tilde{t}}\cos(\tilde{\Omega}_0\tilde{t}+\phi), \end{aligned} \tag{13}$$

where

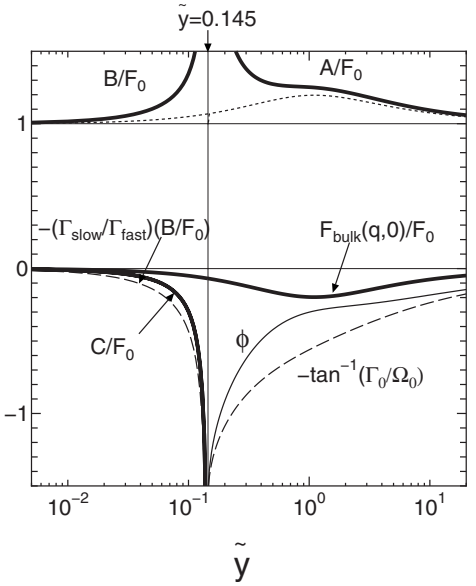

FIG. 3. Various parameters describing the shape of the correlation function $F(q,t)$ in the damped oscillator regime ($\tilde{y}>0.145$) and the overdamped regime ($\tilde{y}<0.145$). The thick solid lines indicate normalized amplitudes A/F_0, B/F_0, C/F_0, and $F_{\text{bulk}}(q,0)/F_0$ of F_{osc}, F_{slow}, F_{fast}, and F_{bulk}, respectively. The thin solid line indicates phase shift ϕ of F_{osc}, and the dotted line is the intensity of the ordinary oscillator terms at $t=0$, $A\cos\phi/F_0$ for $\tilde{y}>0.145$ and $(B+C)/F_0$ for $\tilde{y}<0.145$. The dashed lines represent $-(\Gamma_{\text{slow}}/\Gamma_{\text{fast}})(B/F_0)$ and $-\tan^{-1}(\Gamma_0/\omega_0)$, which are expected to coincide with C/F_0 and ϕ, respectively, in the approximation ignoring the bulk shear mode.

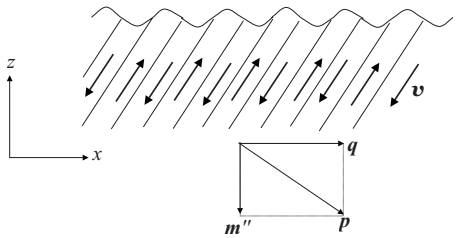

FIG. 4. A schematic drawing of a bulk shear mode with a wave vector $\boldsymbol{p}=(q,0,m'')$ and a velocity vector $\boldsymbol{v}$.

$$A=\left|\frac{2F_0\tilde{y}}{\tilde{\omega}(d\tilde{D}/d\tilde{\omega})}\right|_{\tilde{\omega}=\pm\tilde{\Omega}_0-i\tilde{\Gamma}_0}=\left|\frac{2F_0\tilde{y}}{i\tilde{\omega}\left[2(1-i\tilde{\omega})-\frac{1}{\sqrt{1-2i\tilde{\omega}}}\right]}\right|_{\tilde{\omega}=\pm\tilde{\Omega}_0-i\tilde{\Gamma}_0}, \tag{14}$$

$$\phi=\mp\arg\left(\frac{1}{\tilde{\omega}(d\tilde{D}/d\tilde{\omega})}\right)_{\tilde{\omega}=\pm\tilde{\Omega}_0-i\tilde{\Gamma}_0}=\mp\arg\left(\frac{1}{i\tilde{\omega}\left[2(1-i\tilde{\omega})-\frac{1}{\sqrt{1-2i\tilde{\omega}}}\right]}\right)_{\tilde{\omega}=\pm\tilde{\Omega}_0-i\tilde{\Gamma}_0} \tag{15}$$

are the amplitude and the phase of the oscillation term, respectively.

(ii) In the over damped region ($\tilde{y}<0.145$), the integrals around C_0 and C_1 give exponentially damping functions with dimensionless damping rates $\tilde{\Gamma}_{\text{slow}}$ and $\tilde{\Gamma}_{\text{fast}}$, respectively. We denote these functions by $F_{\text{slow}}(q,t)$ and $F_{\text{fast}}(q,t)$,

$$F_{\text{slow}}(q,t)+F_{\text{fast}}(q,t)=-F_0\tilde{y}\left(\int_{C_0}+\int_{C_1}\right)d\tilde{\omega}\frac{e^{-i\tilde{\omega}\tilde{t}}}{2\pi i\tilde{\omega}\tilde{D}}=\left.\frac{F_0\tilde{y}e^{-i\tilde{\omega}\tilde{t}}}{\tilde{\omega}(d\tilde{D}/d\tilde{\omega})}\right|_{\tilde{\omega}=-i\tilde{\Gamma}_{\text{slow}}}+\left.\frac{F_0\tilde{y}e^{-i\tilde{\omega}\tilde{t}}}{\tilde{\omega}(d\tilde{D}/d\tilde{\omega})}\right|_{\tilde{\omega}=-i\tilde{\Gamma}_{\text{fast}}}=Be^{-\tilde{\Gamma}_{\text{slow}}\tilde{t}}+Ce^{-\tilde{\Gamma}_{\text{fast}}\tilde{t}}, \tag{16}$$

where

$$B=\left.\frac{F_0\tilde{y}}{\tilde{\omega}(d\tilde{D}/d\tilde{\omega})}\right|_{\tilde{\omega}=-i\tilde{\Gamma}_{\text{slow}}}=\frac{F_0\tilde{y}}{\tilde{\Gamma}_{\text{slow}}\left[2(1-\tilde{\Gamma}_{\text{slow}})-\frac{1}{\sqrt{1-2\tilde{\Gamma}_{\text{slow}}}}\right]}, \tag{17}$$

$$C=\left.\frac{F_0\tilde{y}}{\tilde{\omega}(d\tilde{D}/d\tilde{\omega})}\right|_{\tilde{\omega}=-i\tilde{\Gamma}_{\text{fast}}}=\frac{F_0\tilde{y}}{\tilde{\Gamma}_{\text{fast}}\left[2(1-\tilde{\Gamma}_{\text{fast}})-\frac{1}{\sqrt{1-2\tilde{\Gamma}_{\text{fast}}}}\right]} \tag{18}$$

are the amplitudes of the slow and the fast damping modes, respectively.

The $\tilde{y}$ dependence of the parameters A/F_0 and ϕ in the damped oscillator regime and B/F_0 and C/F_0 in the overdamped regime are depicted in Fig. 3. The amplitude of the fast mode C gives negative contribution in the overdamped region. Presence of the fast mode near the critical damping is confirmed experimentally by Hoshino *et al.* [11]. When $\tilde{y}$ is approached to the critical value 0.145, the normalized amplitudes A/F_0, B/F_0, and $|C|/F_0$ increase sharply. However, the values of the ordinary oscillator terms at $t=0$, $F_{\text{osc}}(q,0)/F_0=A\cos\phi/F_0$ and $[F_{\text{slow}}(q,0)+F_{\text{fast}}(q,0)]/F_0=(B+C)/F_0$, remain nearly unity as indicated by the dotted line.

C. Bulk shear-mode term

Next, we focus our attention on the integral along the path C_2, which corresponds to the bulk shear mode as seen below. We denote the term by $F_{\text{bulk}}(q,t)$. It comes from the discontinuity of $\tilde{D}(\tilde{y},\tilde{\omega})$ across the branch cut,

$$\begin{aligned}
F_{\text{bulk}}(q,t) &= -F_0\tilde{y}\int_{C_2} d\tilde{\omega}\frac{e^{-i\tilde{\omega}\tilde{t}}}{2\pi i\tilde{\omega}\tilde{D}} \\
&= -F_0\tilde{y}\int_{1/2}^{\infty}\frac{d\tilde{\gamma}e^{-\tilde{\gamma}\tilde{t}}}{2\pi i\tilde{\gamma}} \\
&\quad\times\left(\frac{1}{\tilde{D}(\tilde{y},-i\tilde{\gamma}+\epsilon)}-\frac{1}{\tilde{D}(\tilde{y},-i\tilde{\gamma}-\epsilon)}\right) \\
&= -F_0\tilde{y}\int_{1/2}^{\infty}d\tilde{\gamma}\frac{e^{-\tilde{\gamma}\tilde{t}}}{2\pi i\tilde{\gamma}}\left(\frac{1}{-i\sqrt{2\tilde{\gamma}-1}-(1-\tilde{\gamma})^2-\tilde{y}}-\frac{1}{i\sqrt{2\tilde{\gamma}-1}-(1-\tilde{\gamma})^2-\tilde{y}}\right) \\
&= -\frac{F_0\tilde{y}}{\pi}\int_{1/2}^{\infty}d\tilde{\gamma}\frac{e^{-\tilde{\gamma}\tilde{t}}\sqrt{2\tilde{\gamma}-1}}{\tilde{\gamma}\{[(1-\tilde{\gamma})^2+\tilde{y}]^2+(2\tilde{\gamma}-1)\}} \\
&\equiv -\int_{1/2}^{\infty}d\tilde{\gamma}g(\tilde{\gamma})e^{-\tilde{\gamma}\tilde{t}}. \qquad (19)
\end{aligned}$$

This form has already been given by Nelkin [13]. However, he wrote about this term only briefly, and, to our knowledge, this formula has never been used for the analysis of experimental data. Therefore, it is worth examining the formula containing this term more closely. From the experimental point of view, it is important to study the actual time dependence of the term, and to examine how the intensity of the term depends on the liquid parameters.

It should be noted that F_{bulk} is a superposition of exponential type damping modes $e^{-\tilde{\gamma}\tilde{t}}$ with a weight $-g(\tilde{\gamma})$. The shaded area in Fig. 1 ($\tilde{\gamma}>1/2$) indicates the distribution of the dimensionless damping rates $\tilde{\gamma}$, which contribute to integral (19). This exponential damping corresponds to the pure imaginary frequency $\tilde{\omega}=-i\tilde{\gamma}$. Substituting this imaginary frequency in Eq. (3), it is noticed that $m=q\sqrt{1-2i\tilde{\omega}}=q\sqrt{1-2\tilde{\gamma}}=im''$ becomes purely imaginary for $\tilde{\gamma}>1/2$. The velocity $\boldsymbol{v}$ behaves as $\boldsymbol{v}=(v_x,v_y,v_z)\propto(-m'',0,q)\exp[i(qx+m''z)-\gamma t]$ when $|z|\gg q^{-1}$. This mode can be interpreted as a bulk shear mode with a wave vector $\boldsymbol{p}=(q,0,m'')$, which is illustrated schematically in Fig. 4. The velocity vector $\boldsymbol{v}$ is perpendicular to the wave vector $\boldsymbol{p}$, and the dimensioned damping rate $\gamma=(2\eta q^2/\rho)\tilde{\gamma}=(\eta/\rho)(q^2+m''^2)$ coincides precisely with the damping rate $(\eta/\rho)p^2$ of the bulk shear mode with wave number p.

As shown in Appendix, the integration in Eq. (19) can be executed analytically,

$$\begin{aligned}
F_{\text{bulk}}(q,t) = -F_0\tilde{y}\sum_{i=0}^{3}\frac{a_i}{\tilde{\gamma}_i}\Bigg\{&\text{erfc}\left(\sqrt{\frac{\tilde{t}}{2}}\right) \\
&-\sqrt{1-2\tilde{\gamma}_i}e^{-\tilde{\gamma}_i\tilde{t}}\,\text{erfc}\left(\sqrt{\frac{\tilde{t}}{2}(1-2\tilde{\gamma}_i)}\right)\Bigg\}. \qquad (20)
\end{aligned}$$

Here, $\text{erfc}(x)$ is the Gauss's error function

$$\text{erfc}(x)=\frac{2}{\sqrt{\pi}}\int_x^{\infty}e^{-t^2}dt,$$

and $\tilde{\gamma}_i$ and a_i ($i=0\sim3$) are defined by Eqs. (A1a)–(A1c) and (A3).

The total autocorrelation function $F(q,t)$ of CW is expressed by the sum of the ordinary oscillator terms and the bulk shear-mode term,

$$F(q,t)=\begin{cases}F_{\text{osc}}(q,t)+F_{\text{bulk}}(q,t)=Ae^{-\Gamma_0 t}\cos(\Omega_0 t+\phi)+F_{\text{bulk}}(q,t), & (\tilde{y}>0.145)\\ F_{\text{slow}}(q,t)+F_{\text{fast}}(q,t)+F_{\text{bulk}}(q,t)=Be^{-\Gamma_{\text{slow}}t}+Ce^{-\Gamma_{\text{fast}}t}+F_{\text{bulk}}(q,t), & (\tilde{y}<0.145).\end{cases} \qquad (21)$$

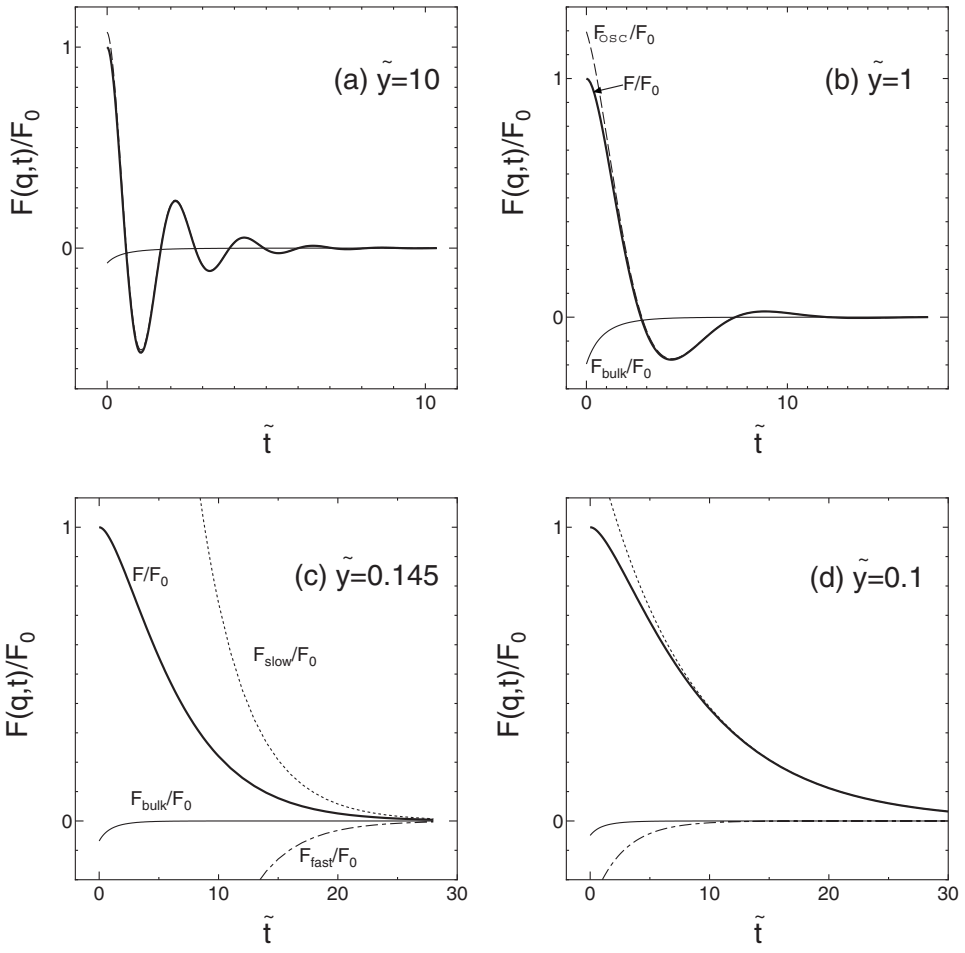

FIG. 5. The thick solid lines indicate the normalized correlation functions $F(q,t)/F_0$ at (a) $\tilde{y}=10$ and (b) $\tilde{y}=1$ (damped oscillator regime) and (c) $\tilde{y}=0.145$ (critical damping regime) and at (d) $\tilde{y}=0.1$ (overdamped regime). The dashed, dotted, chain, and thin solid lines represent the contributions of $F_{\mathrm{osc}}(q,t)/F_0$, $F_{\mathrm{slow}}(q,t)/F_0$, $F_{\mathrm{fast}}(q,t)/F_0$ and $F_{\mathrm{bulk}}(q,t)/F_0$, respectively.

The parameters A, ϕ, B, and C are given in Eqs. (14), (15), (17), and (18), respectively, and the bulk shear term $F_{\mathrm{bulk}}(q,t)$ is calculated by Eq. (20).

Figure 5 shows the normalized correlation functions $F(q,t)/F_0$ at (a) $\tilde{y}=10$ and (b) $\tilde{y}=1$ (damped oscillator regime) and (c) $\tilde{y}=0.145$ (critical damping regime) and at (d) $\tilde{y}=0.1$ (overdamped regime). The dashed, dotted, chain, and thin solid lines represent the contributions of $F_{\mathrm{osc}}(q,t)/F_0$, $F_{\mathrm{slow}}(q,t)/F_0$, $F_{\mathrm{fast}}(q,t)/F_0$, and $F_{\mathrm{bulk}}(q,t)/F_0$, respectively. $F_{\mathrm{bulk}}(q,t)$ appears in small $\tilde{t}$ region and gives negative contribution to $F(q,t)$. In Figs. 5(a), 5(c), and 5(d), it is found that $|F_{\mathrm{bulk}}|$ is quite small and negligible. However, at $\tilde{y}=1$ [Fig. 5(b)], $|F_{\mathrm{bulk}}|$ becomes large, and relatively large deviation of $F(q,t)$ from $F_{\mathrm{osc}}(q,t)$ is observed below $\tilde{t}\leq 1$.

$\tilde{y}$ dependence of the contribution of the bulk shear mode at $t=0$, $F_{\mathrm{bulk}}(q,0)/F_0$, is shown in Fig. 3. In a wide range of $\tilde{y}$, $|F_{\mathrm{bulk}}(q,0)/F_0|$ is negligibly small. However, it shows a broad maximum around $\tilde{y}\sim 1$, where the contribution of $|F_{\mathrm{bulk}}(q,0)|$ becomes $\sim 20\%$ of F_0, and F_{bulk} cannot be ignored in this area.

It may be interesting to study how the bulk shear mode affects the time derivative of $F(q,t)$ in the small t region. Since a time-correlation function such as $F(q,t)$ is independent of the choice of time origin and invariant under time translation, the following equation is derived [14]:

$$\left.\frac{\partial F}{\partial t}\right|_{t=0}=0. \tag{22}$$

Substituting the Eq. (21) into Eq. (22), one obtains

$$-A(\Omega_0 \sin\phi+\Gamma_0\cos\phi)+dF_{\mathrm{bulk}}/dt=0 \quad (\tilde{y}>0.145),$$

$$-B\Gamma_{\mathrm{slow}}-C\Gamma_{\mathrm{fast}}+dF_{\mathrm{bulk}}/dt=0 \quad (\tilde{y}<0.145).$$

When the bulk shear mode is ignored, the following relations are obtained:

$$\phi=-\tan^{-1}(\Gamma_0/\omega_0) \quad (\tilde{y}>0.145),$$

$$C=-(\Gamma_{\mathrm{slow}}/\Gamma_{\mathrm{fast}})B \quad (\tilde{y}<0.145).$$

The dashed lines in Fig. 3 represent $-\tan^{-1}(\Gamma_0/\omega_0)$ and $-(\Gamma_{\mathrm{slow}}/\Gamma_{\mathrm{fast}})(B/F_0)$, which are expected to coincide with ϕ and C/F_0, respectively, in the approximation ignoring the bulk shear mode. In the damped oscillation region, it is found that ϕ deviates significantly from $-\tan^{-1}(\Gamma_0/\omega_0)$ around $\tilde{y}\sim 1$, where contribution of F_{bulk} becomes important. Near the critical damping ($\tilde{y}\sim 0.145$), C/F_0 nearly coincides with $-(\Gamma_{\mathrm{slow}}/\Gamma_{\mathrm{fast}})(B/F_0)$ because $F_{\mathrm{bulk}}(q,0)$ is small in this region compared to B and C. This is the reason why the experimental overdamped CW data near the critical damping can well be explained without taking into account the bulk

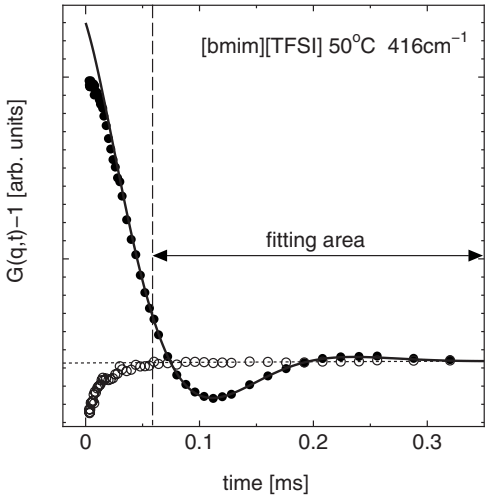

FIG. 6. The closed circles indicate a representative result of the observed autocorrelation function $G(q,t)-1$ at $T=50$ °C and $q=416$ cm^{-1} for [bmim][TFSI]. The solid line is the fitting curve using a simple damped oscillation function [Eq. (23)], and the dotted line is the base line. The fitting area is indicated by the arrow. The open circles are the difference between the observed data and the fitting curve, corresponding to the bulk shear mode.

shear-mode contribution as shown in the previous paper [11]. In the region $\tilde{y} \leq 0.1$, the deviation gets larger again because the amplitude of the fast mode C becomes small and $F_{\mathrm{bulk}}(q,0)$ cannot be ignored compared to C.

III. COMPARISON WITH EXPERIMENTAL DATA

A. Experimental procedure

We performed SDLS measurements on the surface of an IL, [bmim][TFSI]. A high-purity [bmim][TFSI] sample was purchased from Kanto Chemical Co., Inc. The liquid sample was enclosed in a quartz cell with diameter of 50 mm. The cell was evacuated using a rotary pump and a liquid nitrogen trap, and the measurements were performed under vacuum conditions.

We used a He-Ne laser (1.5mW, wavelength $\lambda=632.8$ nm) as a light source. The light scattered by the capillary waves was detected by a photomultiplier through a pinhole (0.5mm in diameter) and an optical fiber.

Together with the scattering from the liquid surface, the light scattered from the surfaces of optical elements is optically mixed at the detector. The latter acts as the reference light or the local oscillator to fulfill the necessary conditions for optical heterodyning. From the output signal of the detector, $I(q,t)$, the time-autocorrelation function $G(q,t)=\langle I(q,t)I(q,0)\rangle/\langle I\rangle^2$ was calculated with a multiple-tau digital autocorrelator ALV-610/160. In general, the autocorrelation function $G(q,t)$ can be expressed as a combination of heterodyne and homodyne terms [15]. The heterodyne component of $G(q,t)-1$ is proportional to the correlation function of the CW, $F(q,t)$. In the present case, the heterodyne term is dominant because the reference signal is much more intense compared to the scattering from the CW. In the following analysis, we ignore the homodyne contribution.

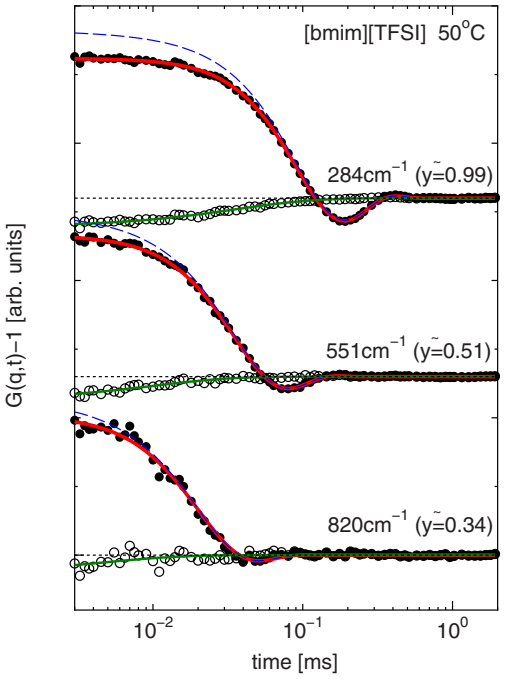

FIG. 7. (Color online) The closed circles indicate the observed autocorrelation functions $G(q,t)-1$ at $T=50$ °C and at various wave numbers for [bmim][TFSI]. The thick solid lines are the full theoretical correlation functions [Eq. (25)]. The dashed and thin solid lines are the contributions of the ordinary damped oscillator term $G_0F^{\rho}_{\mathrm{osc}}$ and the bulk shear term $G_0F^{\rho}_{\mathrm{bulk}}$, respectively. The dotted lines are the base lines. The open circles are the difference between the observed data and $G_0F^{\rho}_{\mathrm{osc}}$ term, corresponding to the bulk shear term.

We deduced the surface tension and the viscosity from the SDLS data by using the curve-fitting method described in a pervious paper [9]. In this method, the experimentally obtained power spectrum is fitted by the strict theoretical expression of power spectrum (5). In this calculation, we also adopted a global fitting procedure. Namely, many spectra taken at various wave numbers at the same temperature condition were fitted simultaneously while sharing the same fitting parameters between data sets.

Detail of the experimental procedure has been given in the pervious paper [9].

B. Results and discussion

The closed circles in Fig. 6 indicate a representative result of the observed autocorrelation function $G(q,t)-1$ at $T=50$ °C and $q=416$ cm^{-1}. At this temperature, the surface tension σ and the viscosity η, which are obtained by the fitting method described in the previous subsection, are 33.2 ± 0.4 mN/m and 20.4 ± 0.6 mPa·s, respectively, and the literature value of the density ρ is 1.42 g/cm^3 [16]. From these parameters, $\tilde{y}$ for the data of Fig. 6 is calculated to be 0.68 ± 0.04, where large contribution of the bulk shear mode is expected.

In order to detect the difference between the observed correlation function and the simple damped oscillator, we

first performed curve-fitting analysis by a simple damped oscillator form

$$G_{\rm osc}(q,t) - 1 = G_0 e^{-\Gamma_0 t} \cos(\Omega_0 t + \phi) + (\text{base line}). \tag{23}$$

Here, G_0 is the intensity factor, and the base line term corresponds to small low frequency fluctuations of the liquid surface induced by the external vibrations. In this calculation, the fitting area is restricted to $t > 0.06$ ms, as indicated by the arrow in Fig. 6. In this fitting area, the contribution of the bulk shear mode is expected to be negligible. The solid line is the fitting curve. The fitting curve and the experimental data points agree well in the fitting area. The obtained angular frequency $\Omega_0 = 25$ ms^{-1} and the damping rate $\Gamma_0 = 18$ ms^{-1} are in good agreement with those calculated from the theoretical dispersion relation, $\Omega_0 = 25.4 \pm 0.6$ ms^{-1} and $\Gamma_0 = 18.9 \pm 0.3$ ms^{-1}. The phase shift $\phi = -0.3$ obtained from the fitting is also close to the theoretical prediction (the thin solid line in Fig. 3), -0.35 ± 0.01. On the other hand, it is larger than the prediction of the approximate theory, which ignores the bulk shear-mode contribution (the dashed line in Fig. 3), $\phi \simeq -\tan^{-1}(\Gamma_0/\Omega_0) = -0.62$. This result implies the presence of the bulk shear mode.

In the short-time region below the fitting area, it is observed that the fitting curve deviates upward compared to the experimental data. The open circles are the difference between the observed data and the fitting curve. Their overall shape is very close to that predicted theoretically for $F_{\rm bulk}$ as shown in Fig. 5(b), and it is concluded that they corresponds to the bulk shear-mode term. To our knowledge, this is the first direct observation of the bulk shear-mode contribution to the CW autocorrelation function.

On the other hand, if one performs curve fitting using the data in the whole time range, the fitting parameter Ω_0 deviates significantly from the theoretical dispersion relation. For example, in the case of Fig. 6, $\Omega_0 = 28$ ms^{-1} is obtained from the fitting in the whole time range, and it is different from the theoretical value of 25.4 ± 0.6 ms^{-1}. This result means that the curve fitting ignoring the bulk shear-mode contribution gives biased values for Ω_0. Therefore, the incorporation of the bulk shear term is crucial for the purpose of obtaining the unbiased values for Ω_0.

Next, we calculated full theoretical correlation function [Eq. (21)] and compared it with the experimental data. In this calculation, we used σ and η obtained by the frequency-domain fitting method described in the previous subsection, and we also used the literature values for ρ [16]. We took into account the instrumental q-resolution function with the standard deviation $\beta \sim 40$ cm^{-1},

$$\rho(q,Q) = \frac{1}{\sqrt{\pi}\beta} \exp[-(Q-q)^2/\beta^2]. \tag{24}$$

Then $G(q,t)$ is written in the form

$$\begin{aligned} G(q,t) - 1 &= \int dQ \rho(q,Q) G_0 [F_{\rm osc}(Q,t) + F_{\rm bulk}(Q,t)] \\ &\quad + (\text{base line}) \\ &= G_0 [F^{\rho}_{\rm osc}(q,t) + F^{\rho}_{\rm bulk}(q,t)] + (\text{base line}), \end{aligned} \tag{25}$$

where $F^{\rho}_{\rm osc}$ and $F^{\rho}_{\rm bulk}$ correspond to $F_{\rm osc}$ and $F_{\rm bulk}$ broadened by $\rho(q,Q)$, respectively, and G_0 is the intensity factor. We used the following approximation for $F^{\rho}_{\rm osc}$ and $F^{\rho}_{\rm bulk}$:

$$\begin{aligned} F^{\rho}_{\rm osc}(q,t) &= \int dQ \rho(q,Q) F_{\rm osc}(Q,t) \\ &\simeq \int dQ \rho(q,Q)[A + A'(Q-q)] \exp\{-[\Gamma_0 + \Gamma_0'(Q-q)]t\} \cos\{[\Omega_0 + \Omega_0'(Q-q)]t + \phi + \phi'(Q-q)\} \\ &= \exp\left\{-\Gamma_0 t - \frac{\beta^2}{4}[(\Omega_0' t + \phi')^2 - (\Gamma_0' t)^2]\right\} \left\{\left(A - \frac{\beta^2}{2} A' \Gamma_0' t\right) \cos\left[\Omega_0 t + \phi - \frac{\beta^2}{2}\Gamma_0' t(\Omega_0' t + \phi')\right]\right. \\ &\quad \left. - \frac{\beta^2}{2} A'(\Omega_0' t + \phi') \sin\left[\Omega_0 t + \phi - \frac{\beta^2}{2}\Gamma_0' t(\Omega_0' t + \phi')\right]\right\}, \end{aligned} \tag{26}$$

$$\begin{aligned} F^{\rho}_{\rm bulk}(q,t) &= \int dQ \rho(q,Q) F_{\rm bulk}(Q,t) \\ &\simeq F_{\rm bulk}(q,t) + \frac{\beta^2}{4} F''_{\rm bulk}(q,t). \end{aligned} \tag{27}$$

Here, the primes indicate partial differentiation with respect to q. This correction becomes important for the small q region below 400 cm^{-1}.

Figure 7 shows the results. The observed data is well explained by the sum of $G_0 F^{\rho}_{\rm osc}$ and $G_0 F^{\rho}_{\rm bulk}$. It should be noted that we used no adjustable parameters except for the intensity factor G_0 and the base line.

The open circles indicate the difference between the observed data and $G_0 F^{\rho}_{\rm osc}$. They are well explained by $G_0 F^{\rho}_{\rm bulk}$

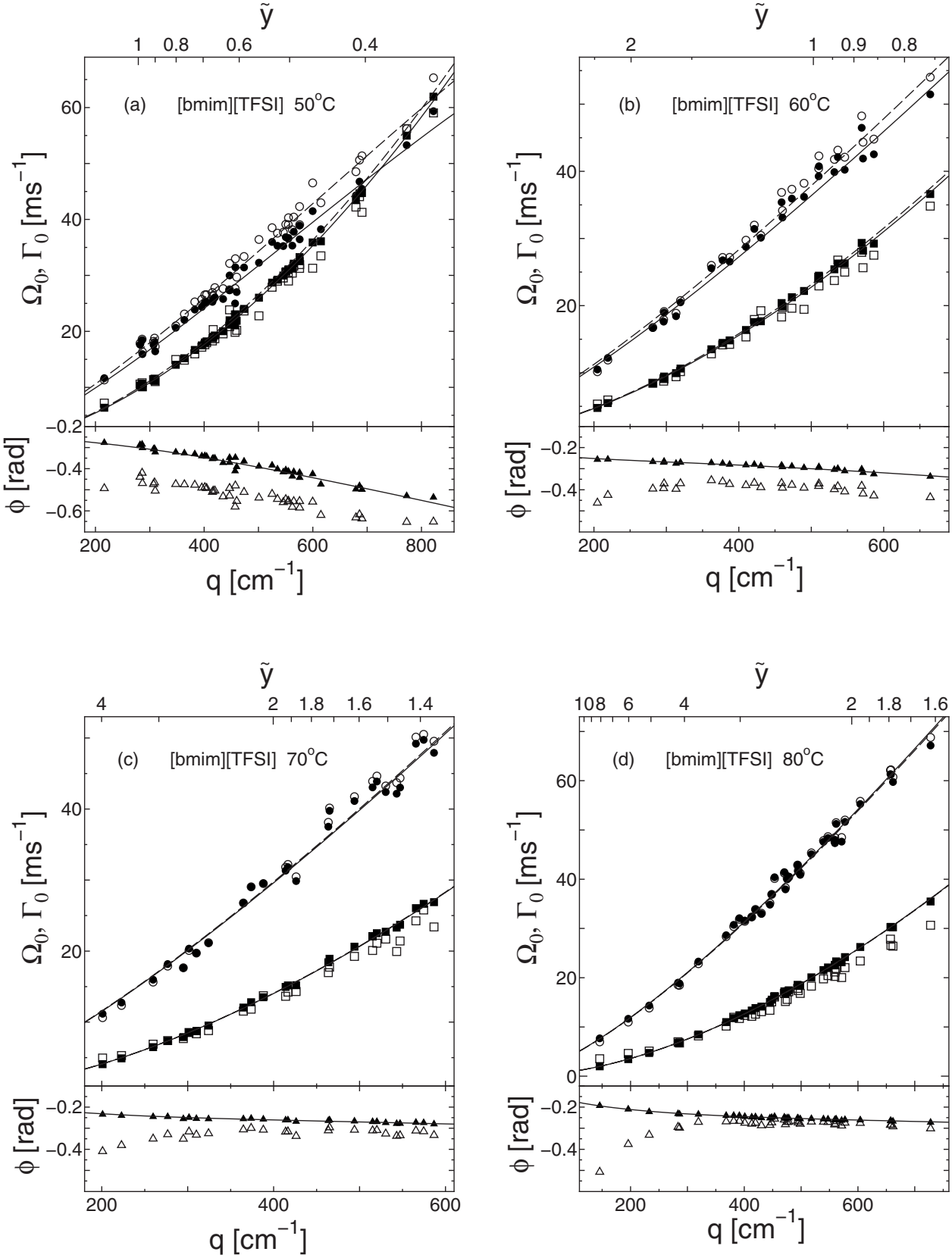

FIG. 8. The wave number q dependence of the frequency Ω_0 (circles), the damping rate Γ_0 (squares), and the phase shift ϕ (triangles) for [bmim][TFSI] at (a) 50 °C, (b) 60 °C, (c) 70 °C, and (d) 80 °C. The solid symbols are calculated using the full theoretical correlation function [Eq. (25)–(27)], and the open symbols are obtained from the simple damped oscillator fitting [Eq. (23)]. The solid lines are the theoretical dispersion curves, and the dashed lines are the fitting curves to the open symbols using Eq. (4).

(the thin solid lines) down to $t \sim 3$ μs. This result indicates that the assumption of incompressible Newtonian liquid is well satisfied for [bmim][TFSI] in the observed time region.

In the previous works [9,11], we obtained the dispersion curves of CW on the surface of [bmim][TFSI] only in the low- and high-temperature regions where the F_{bulk} term is negligible. Now, we are in the position where we can obtain the dispersion curves even in the medium temperature region by using the precise formula for the CW correlation function. Figure 8 shows the q dependence of the frequency Ω_0 (circles), the damping rate Γ_0 (squares), and the phase shift ϕ (triangles) for [bmim][TFSI] at (a) 50 °C, (b) 60 °C, (c) 70 °C, and (d) 80 °C. The data used in this calculation are the same as used in the previous paper [9]. The solid symbols are those calculated using the full theoretical correlation function [Eq. (25)–(27)]. In this calculation, we used σ for each q as free parameters and η is fixed to the values obtained from the method described in the previous subsection. ρ is also fixed to the literature values [16]. Then Ω_0, Γ_0, and ϕ were calculated for each data points from these liquid parameters. They coincide well with the theoretical dispersion curves indicated by the solid lines. On the other hand, the open symbols are Ω_0, Γ_0, and ϕ calculated from the simple damped oscillator fitting [Eq. (23)] ignoring the F_{bulk} term. Unlike the curve-fitting analysis shown in Fig. 6, we used all the data in the whole time range in this calculation. As shown in Fig. 8, this calculation gives larger Ω_0 and smaller Γ_0 than the theoretical curves. It is also found that the phase shift ϕ deviate significantly from the theoretical curves. When the temperature is increased above 70 °C [Figs. 8(c) and 8(d)], these discrepancies become smaller [17] because $\tilde{y}$ becomes larger than unity in the q region of the measurement and contribution of the F_{bulk} term becomes small. This increase of $\tilde{y}$ is mainly due to the strong decrease in η with temperature.

In order to demonstrate the difference between these two sets of dispersion curves, we compared the surface tension σ calculated from these Ω_0 and Γ_0 by curve-fitting method using Eq. (4). In Fig. 8, the fitting curves to the open symbols are indicated by the dashed lines. Figure 9 shows the obtained σ at various temperatures. The solid and the open circles in Fig. 9 correspond to the solid and the open symbols in Fig. 8, respectively. In this calculation, η and ρ are fixed as in the case of the calculation of Fig. 8. The crosses in Fig. 9 are σ calculated by the frequency-domain global fitting method [9], and the solid line is the linear fit to them. The solid circles coincide well with the crosses, while the open circles show deviation around 40 ~ 50 °C, where the contribution of the bulk shear mode becomes important. It is expected that more accurate values of σ and η will be obtained if one uses not only Ω_0 and Γ_0 but the other information contained in the time-domain data, such as the phase shift ϕ and the shape parameters for F_{bulk}. In addition, the global fitting method in the time-domain analysis will be useful for the accurate estimate of the liquid parameters. The efficiency of the global fitting method in the frequency-domain analysis has been proven in the previous paper [9].

An intriguing open question is to what extent the CWs on ILs can be explained by the assumption of incompressible Newtonian liquid. Although no significant deviation from Newtonian fluids is observed in this work, non-Newtonian behavior is evidenced for bulk ILs with long alkyl chains by ultrasonic spectroscopy [18]. At such high frequencies ($\geq$10 MHz) and at low temperatures, CWs on ILs would exhibit non-Newtonian behavior.

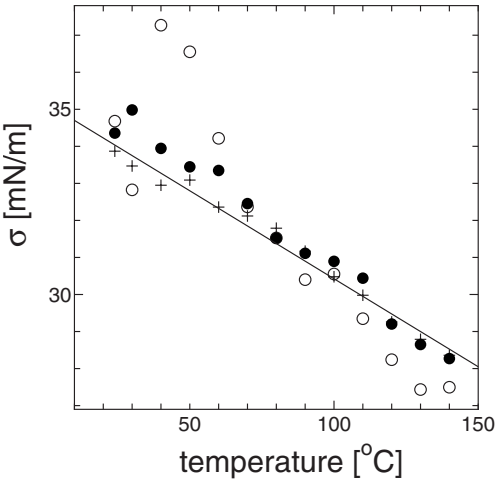

FIG. 9. The surface tension σ at various temperatures calculated from the dispersion curves Ω_0 and Γ_0 in Fig. 8. The solid and open circles correspond to the solid and the open symbols in Fig. 8, respectively. The crosses are σ calculated by the frequency-domain global fitting method [9], and the solid line is the linear fit to them.

We are now planning to extend the present method to the non-Newtonian fluids described by, for example, the Maxwell's model. On the surface of the non-Newtonian fluids, the bulk shear mode is expected to show oscillatory time dependence [4]. From the frequency and the damping rate of the bulk shear mode, it may be possible to obtain viscoelastic properties of the non-Newtonian fluids.

IV. CONCLUSION

In the present work, we indicated that the autocorrelation function of the CW displacement is expressed by the sum of the ordinary oscillator and the bulk-shear-mode terms. The former is expressed by a simple damped oscillator form or a sum of exponentially damping functions depending on the extent of damping. The latter is also written by a superposition of exponentially damping modes, and an analytically exact formula is obtained. We compared the theoretical expression with the SDLS experimental data obtained on the surface of an IL, [bmim][TFSI]. We confirmed that the experimental data is well explained by the theoretical autocorrelation function. Especially, the bulk-shear-mode contribution is observed for the first time.

It is expected that this functional form of the autocorrelation function can be used for precise determination of the liquid parameters such as the surface tension σ and the viscosity η by curve fitting in the time domain.

ACKNOWLEDGMENTS

This work is partially supported by the Grant-in-Aid for Scientific Research on Priority Area "Soft matter Physics"

and "Science of Ionic Liquids" from Ministry of Education, Culture, Sports, Science and Technology, Japan (MEXT), and by a Grant-in-Aid for Scientific Research (Grant No. 20540396) from MEXT.

APPENDIX: DERIVATION OF BULK-SHEAR-MODE CORRELATION FUNCTION [EQ. (20)]

In this appendix, we explain the derivation of analytic form of bulk shear mode correlation function (20) from integral (19).

We start from the fact that the denominator of $g(\tilde{\gamma})$ can be factorized as $[(1-\tilde{\gamma})^2+\tilde{y}]^2+(2\tilde{\gamma}-1)=\Pi_{i=0}^{3}(\tilde{\gamma}-\gamma_i)$. Here, $\tilde{\gamma}_i$ $(i=0\sim3)$ are the roots of the equation $[(1-\tilde{\gamma})^2+\tilde{y}]^2+(2\tilde{\gamma}-1)=0$. Two of the four roots, $\tilde{\gamma}_0$ and $\tilde{\gamma}_1$, are obtained from the roots of dispersion relation (10), $\tilde{\omega}_0$ and $\tilde{\omega}_1$ as

$$\tilde{\gamma}_0 = -i\tilde{\omega}_0, \tag{A1a}$$

$$\tilde{\gamma}_1 = -i\tilde{\omega}_1. \tag{A1b}$$

Other two roots $\tilde{\gamma}_2$ and $\tilde{\gamma}_3$ are calculated from $\tilde{\gamma}_0$ and $\tilde{\gamma}_1$ by

$$\tilde{\gamma}_2, \tilde{\gamma}_3 = -\left(\frac{\tilde{\gamma}_0+\tilde{\gamma}_1}{2}-2\right) \pm \sqrt{\left(\frac{\tilde{\gamma}_0+\tilde{\gamma}_1}{2}-2\right)^2 - \frac{\tilde{y}(\tilde{y}+2)}{\tilde{\gamma}_0\tilde{\gamma}_1}}. \tag{A1c}$$

Using this factorization, the integration in Eq. (19) can be executed in the following way:

$$F_{\mathrm{bulk}}(q,t) = -\frac{F_0\tilde{y}}{\pi}\int_{1/2}^{\infty}\frac{d\tilde{\gamma}e^{-\tilde{\gamma}\tilde{t}}\sqrt{2\tilde{\gamma}-1}}{\tilde{\gamma}\prod_{i=0}^{3}(\tilde{\gamma}-\tilde{\gamma}_i)} = -\frac{F_0\tilde{y}}{\pi}\sum_{i=0}^{3}a_i\int_{1/2}^{\infty}\frac{d\tilde{\gamma}e^{-\tilde{\gamma}\tilde{t}}\sqrt{2\tilde{\gamma}-1}}{\tilde{\gamma}(\tilde{\gamma}-\tilde{\gamma}_i)} = -F_0\tilde{y}\sum_{i=0}^{3}\frac{a_i}{\tilde{\gamma}_i}\left\{\mathrm{erfc}\left(\sqrt{\frac{\tilde{t}}{2}}\right)\right.$$
$$\left. -\sqrt{1-2\tilde{\gamma}_i}e^{-\tilde{\gamma}_i\tilde{t}}\,\mathrm{erfc}\left(\sqrt{\frac{\tilde{t}}{2}(1-2\tilde{\gamma}_i)}\right)\right\}. \tag{A2}$$

Here, $\mathrm{erfc}(x)$ is the Gauss's error function

$$\mathrm{erfc}(x) = \frac{2}{\sqrt{\pi}}\int_x^{\infty}e^{-t^2}dt,$$

and the coefficients a_i $(i=0\sim3)$ are defined by

$$a_i = \prod_{j\neq i}\frac{1}{\tilde{\gamma}_i-\tilde{\gamma}_j}, \tag{A3}$$

which satisfy the identity $\Sigma_{i=0}^{3}a_i\Pi_{j\neq i}(\tilde{\gamma}-\tilde{\gamma}_j)=1$.

[1] *Light Scattering by Liquid Surfaces and Complementary Techniques*, edited by D. Langevin (Marcel Dekker, New York, 1992).

[2] V. G. Levich, *Physicochemical Hydrodynamics* (Prentice-Hall, New Jersey, 1962).

[3] H. Lamb, *Hydrodynamics* (Dover, New York, 1945).

[4] J. Jäckle and K. Kawasaki, J. Phys.: Condens. Matter **7**, 4351 (1995).

[5] M. A. Bouchiat and J. Meunier, J. Phys. (Paris) **32**, 561 (1971).

[6] T. Welton, Chem. Rev. (Washington, D.C.) **99**, 2071 (1999).

[7] R. T. Carlin, H. C. De Long, J. Fuller, and P. C. Trulove, J. Electrochem. Soc. **141**, L73 (1994).

[8] P. Wang, S. M. Zakeeruddin, J. E. Moser, and M. Gratzel, J. Phys. Chem. B **107**, 13280 (2003).

[9] Y. Ohmasa, T. Hoshino, R. Osada, and M. Yao, Chem. Phys. Lett. **455**, 184 (2008).

[10] E. Sloutskin, P. Huber, M. Wolff, B. M. Ocko, A. Madsen, M. Sprung, V. Schön, J. Baumert, and M. Deutsch, Phys. Rev. E **77**, 060601(R) (2008).

[11] T. Hoshino, Y. Ohmasa, R. Osada, and M. Yao, Phys. Rev. E **78**, 061604 (2008).

[12] D. Byrne and J. C. Earnshaw, J. Phys. D **12**, 1133 (1979).

[13] M. Nelkin, Phys. Fluids **15**, 1685 (1972).

[14] J. P. Hansen and I. R. McDonald, *Theory of Simple Liquids* (Academic, New York, 1986).

[15] B. J. Berne and R. Pecora, *Dynamic Light Scattering* (Wiley, New York, 1976).

[16] H. Tokuda, K. Ishii, M. A. B. H. Susan, S. Tsuzuki, K. Hayamizu, and M. Watanabe, J. Phys. Chem. B **110**, 2833 (2006).

[17] The deviation of ϕ (open triangles) from the theoretical curve in the low-q region is due to the phase shift which is related to the finite resolution β. This phase shift can be evaluated from Eq. (26).

[18] W. Makino, R. Kishikawa, M. Mizoshiri, S. Takeda, and M. Yao, J. Chem. Phys. **129**, 104510 (2008).